Chinese Chemical Letters 35 (2024) 108346

Contents lists available at ScienceDirect

Chinese Chemical Letters

journal homepage: www.elsevier.com/locate/cclet

# Multifunctional biodegradable nanoplatform based on oxaliplatin prodrug cross-linked mesoporous polydopamine for enhancing cancer synergetic therapy

Ping Sun[a,1], Zimu Li[a,1], Dan Zhang[a,1], Wenfeng Zeng[a], Yi Zheng[b], Lin Mei[a,c], Hongzhong Chen[a,*], Nansha Gao[a,*], Xiaowei Zeng[a,*]

[a] School of Pharmaceutical Sciences (Shenzhen), Sun Yat-sen University, Shenzhen 518107, China
[b] Central Laboratory, University of Chinese Academy of Sciences-Shenzhen Hospital, Shenzhen 518106, China
[c] Tianjin Key Laboratory of Biomedical Materials, Key Laboratory of Biomaterials and Nanotechnology for Cancer Immunotherapy, Institute of Biomedical Engineering, Chinese Academy of Medical Sciences and Peking Union Medical College, Tianjin 300192, China

ARTICLE INFO

*Article history:*
Received 14 January 2023
Revised 13 March 2023
Accepted 16 March 2023
Available online 24 March 2023

*Keywords:*
Oxaliplatin prodrug
Mesoporous polydopamine
Charge reversal
Synergetic therapy
Cancer nanotechnology

ABSTRACT

Due to the limitations of conventional chemotherapy including side effects, poor prognosis, and drug resistance, there is an urgent need for the development of a novel multi-functional combined therapy strategy. Dopamine-modified oxaliplatin prodrug (OXA-DA) was successfully synthesized in this study to ameliorate the organ distribution of oxaliplatin for improving the drug efficacy and reducing toxic side effects, and OXA-DA was applied to develop a porous oxaliplatin cross-linked polydopamine nanoparticle for loading siPD-L1 to construct multifunctional nanoplatform. The multifunctional nanoplatform was modified with poly(2-ethyl-2-oxazoline) (PEOz), which occurred charge reversal in the tumor microenvironment, and exerted the lysosomal escape effect in tumor cells to improve the bioavailability of small interfering RNA targeting programmed cell death-ligand 1 (siPD-L1). The pH-responsive charge reversal, photothermal, biodegradation, lysosomal escape ability, PD-L1 protein degradation, toxicity properties and multiple antitumor effects were comprehensively evaluated *in vitro* and *in vivo* experiments. The findings indicated that OXA-DA-siPD-L1@PDA-PEOz excellently induced tumor cell necrosis and apoptosis as a result of the synergistic effect of chemo-photothermal therapy, and upregulated $CD8^+$ T cells produced interferon-$\gamma$ (IFN-$\gamma$) to further attack the tumor cells. In conclusion, the novel nanoplatform-mediated chemo/photothermal/immunotherapy has promising clinical applications in the treatment of malignant tumors.



Cancer is admittedly a primary threat to human health worldwide, there are approximately 4.82 million and 2.37 million new cancer cases in 2022, and 3.21 million and 0.64 million cancer deaths in China and the USA, respectively [1,2]. There is an urgent need to develop novel anti-tumor strategies that combine chemotherapy with other treatment options due to the several limitations associated with traditional chemotherapy, including side effects, drug resistance and poor prognosis [3–5].

Oxaliplatin (OXA) (II), the most recent internationally recognized platinum derivative for clinical application, demonstrated considerable differences in pharmacology, antitumor activity spectrum and cytotoxicity when compared to cisplatin and carboplatin [6]. OXA (II) is less toxic to the kidneys and bone marrow and exhibits no cross-resistance with other platinum-based anticancer drugs [7,8]. The drawbacks of OXA (II) were overcome in this study by employing the prodrug carboxylated OXA-COOH (IV), this prodrug is less toxic [9–12].

Photothermal therapy (PTT) is a noninvasive strategy for treating various cancers owing to its low systemic toxicity and superior therapeutic effect [13,14], which is usually applied in combination with other cancer treatment techniques including chemotherapy, radiation therapy and immunotherapy [15,16]. Polydopamine (PDA), a melanin-like polymer, has been developed as a promising carrier for drug delivery in cancer therapy due to its intrinsic biocompatibility, high drug loading capacity and strong near-infrared (NIR) absorption enabling PTT [17–21]. Mesoporous polydopamine nanoparticles (MPDA NPs) provide efficient drug encapsulation and

* Corresponding authors.
*E-mail addresses:* chenhzh58@mail.sysu.edu.cn (H. Chen), gaonsh@mail.sysu.edu.cn (N. Gao), zengxw23@mail.sysu.edu.cn (X. Zeng).
[1] These authors contributed equally to this work.

https://doi.org/10.1016/j.cclet.2023.108346
1001-8417/

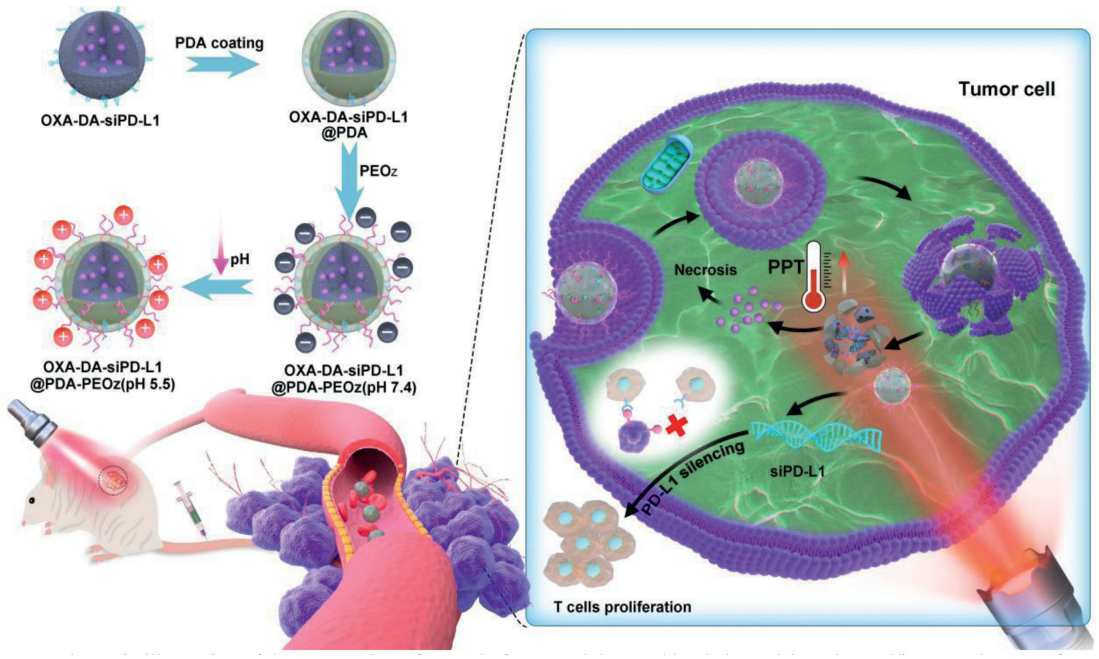


**Fig. 1.** Schematic illustration of the preparation of nanoplatforms and the combined chemo/photothermal/immunotherapy of tumor cells.

photothermal conversion. Despite these marked features, the use of MPDA NPs as theranostic nanoplatforms combining cancer treatment strategies has rarely been reported [22,23].

Poly(2-ethyl-2-oxazoline) (PEOz), owning similar properties to polyethylene glycol such as hydrophilicity, low toxicity, and increased systemic cycle time in the neutral environment, is often used to modify nano-drug delivery systems to enhance their stability [24–27]. It can cause a charge reversal in tumor microenvironments (TME, pH ≈ 6.5) or cell lysosomes (pH ≈ 5.5) for tumor penetration and lysosome escape [28,29].

Cancer immunotherapy has considerably advanced over the past decades. Given the large number of research devoted to advancing endogenous and synthetic immunotherapeutic approaches. The challenges facing cancer immunotherapy include a lack of confidence in translating preclinical findings and determining the optimal combination of immune-based therapies for any particular patient. Addressing these challenges will require the combined efforts of basic researchers and clinicians, as well as the pooling of resources to accelerate the understanding of the complex interactions between cancer and the immune system, and develop improved treatment options for cancer patients [30,31]. The PD-1/PD-L1 pathway and the CTLA-4 pathway constitute the well-known brake system of the immune system [32,33]. Targeting these two pathways is a promising anticancer strategy [34–37].

In this study, dopamine-modified oxaliplatin (OXA-DA) was successfully synthesized and used to crosslink the MPDA NPs for loading small interfering RNA targeting programmed cell death-ligand 1 (siPD-L1). The MPDA NPs were modified with a pH-responsive PEOz and resulted in charge reversal in the TME for enhancing cell internalization. The composite NPs have three advantages in this project: First, oxaliplatin cross-linked dopamine is evenly dispersed within the nanoplatform for improving its biosafety and biodegradability. Oxaliplatin (II) is modified with dopamine to become OXA-DA (IV), which enhances drug efficacy while reducing side effects. Second, PDA has a good photothermal effect and biodegradability. Therefore, it has an excellent photothermal therapy effect and is easy to be degraded *in vivo*. Third, the PEOz-modified nanoplatform is pH-responsive and can achieve lysosome escape in tumor cells, which can improve the bioavailability of siPD-L1. The synthetic process of OXA-DA-siPD-L1@PDA-PEOz nanoparticle was exhibited in Fig. 1.

OXA (II) is a common alkylating agent that exerts cytotoxic effects by inhibiting messenger RNA synthesis and DNA damage. We converted OXA (II) to OXA-COOH (IV), which has lower cytotoxicity and thus can be used at higher doses. As shown in Fig. S1 (Supporting information), two axial hydroxyl groups were added to OXA (II) by a reaction with $H_2O_2$. The hydroxyl groups were then reacted with succinic anhydride to yield a carboxyl group. DA was linked to OXA-COOH (IV) by an amide bond. $^1$H-nuclear magnetic resonance ($^1$H NMR) spectroscopy was used to elucidate the structure of the OXA-COOH (IV) and OXA-DA copolymer. The $^1$H NMR spectra of OXA (II) and OXA-COOH (IV) in DMSO-$d_6$ were illustrated in Fig. S2 (Supporting information). The chemical shifts of solvent and $D_2O$ appeared at 2.5 ppm and 3.3 ppm, respectively. Furthermore, OXA (II) had two characteristic peaks of the -$NH_2$ on cyclohexane at 5.34 ppm (br, 2H) and 6.10 ppm (br, 2H). These two peaks shifted downfield to 6.9–8.6 ppm (br, 4H) in OXA-COOH (IV). The proton peaks of cyclohexane in both compounds were all in the range of 0.7–2.2 ppm (m, 10H). In addition, the peaks at 2.2–2.4 ppm due to -$CH_2$- of succinic acid confirmed the successful synthesis of the OXA-COOH (IV) polymer. While in the $^1$H NMR spectroscopy of OXA-DA copolymer, it is clear that the OXA characteristic peak and dopamine characteristic peak was at the position of 6.9–8.6 ppm (br, 4H) and 6.5–6.8 ppm, indicated that OXA-DA copolymer has been successfully synthesized.

Using the synthesized OXA-DA copolymer as the raw material, porous nanoparticles, namely OXA-DA nanoparticles, were constructed through a polymerization reaction, and oxaliplatin was embedded in the nanoparticle skeleton to increase the drug loading stability. The porous nanoparticles were treated with guanidine hydrochloride to make the surface positively charged, and then the negatively charged siPD-L1 was adsorbed to prepare OXA-siPD-L1 co-loaded composite nanoparticles. Then, a poly-dopamine (PDA) layer was coated on the outside of the nanocomposite system by *in-situ* polymerization of DA to prepare OXA-DA-siPD-L1@PDA composite nanoparticles. Finally, PEOz-$NH_2$ was attached to the surface of the polydopamine coating layer through the Michael reaction, resulting in a pH-responsive charge-reversible

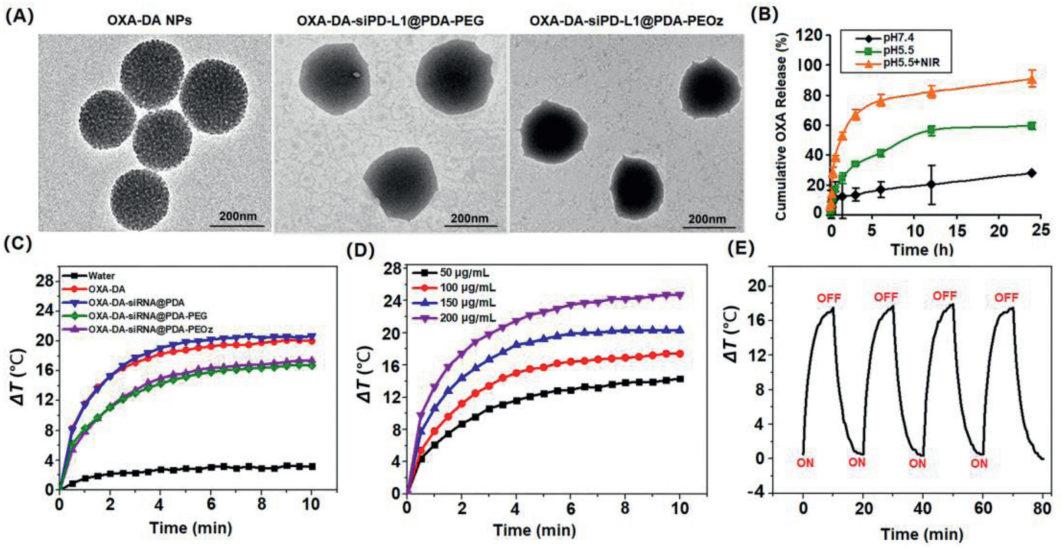


**Fig. 2.** Characterizations of NPs: (A) TEM image of different types NPs; (B) Drug release kinetics of OXA-DA-siPD-L1@PDA-PEOz NPs in pH 7.4, pH 5.5 and pH 5.5 + NIR; (C) Temperature elevation curves OXA-DA-siPD-L1@PDA-PEOz NPs for different power and being irradiated of pure water, OXA-DA, OXA-DA-siPD-L1@PDA, OXA-DA-siPD-L1@PDA-PEG, and OXA-DA-siPD-L1@PDA-PEOz under 808 nm laser irradiation (1.0 W/cm$^2$) for 10 min; (D) Photothermal heating curves of the OXA-DA-siPD-L1@PDA-PEOz NPs for different concentrations and being irradiated with the 808 nm laser (1.0 W/cm$^2$) for 10 min; (E) Heating of a suspension of the OXA-DA-siPD-L1@PDA-PEOz in water for five lasers on/off cycles with an 808 nm NIR laser at a power density of 1.0 W/cm$^2$.

nano-composite delivery system, thus the OXA-DA-siPD-L1@PDA-PEOz nano-composite delivery system was obtained. In the same way, the OXA-DA-siPD-L1@PDA-PEG nano-composite system was prepared as a control group.

In addition, Fourier transform infrared (FTIR) spectroscopy was applied to confirm the structure of nano-composite preparations, the characteristic peak at 3400 cm$^{-1}$ and 1627 cm$^{-1}$ attributed to PDA and PEOz, respectively, indicated the successful construction of PEOz modified oxaliplatin cross-linked dopamine nano-composite delivery system (Fig. S3 in Supporting information). The surface morphology of the nano-composite was observed by transmission electron microscopy (TEM), and the results are shown in Fig. 2A. The pore structure on the surface of the unmodified OXA-DA nanoparticles could be clearly observed, and the pores were evenly distributed with a particle size of about 220 nm. After modification by PEG and PEOz, the surface of OXA-DA-siPD-L1@PDA nanoparticles exhibited an obvious polymer-like coating. The pore structure became less clear, and the particle size increased slightly to about 260–290 nm, indicating the successful coating of PEG and PEOz (Table S1 and Fig. S4 in Supporting information). The average encapsulation efficiency and drug loading of OXA-DA-siPD-L1@PDA-PEOz detected by ultraviolet–visible (UV–vis) spectrophotometer were 88.3% ± 0.28% and 1.58% ± 0.57%, respectively, indicating that the nano-composite system could well carry oxaliplatin. Moreover, oxaliplatin was embedded in the nano-system through chemical bonding, thus further improving the drug stability. The sustained release property of the OXA-DA-siPD-L1@PDA-PEOz nano-composite system under different pH and light conditions was examined and the results are shown in Fig. 2B. When no light was given, the cumulative release of OXA from OXA-DA-siPD-L1@PDA-PEOz nanocomposite system in the medium at pH 5.5 was 50% after 24 h, compared to a cumulative release of only 25.38% in the medium at pH 7.4, which may be attributed to the responsive degradation of PDA in the weak acidic environment, suggesting good pH-responsive drug release property of the PDA layer. Therefore, the nanoformulation is more stable in a near-neutral pH environment, and the drug release increases in a slightly acidic environment. When the OXA-DA-siPD-L1@PDA-PEOz nano-composite system was exposed to a pH 5.5 medium and illuminated with 808 nm near-infrared light (NIR) for a certain period of time at the time of sampling, the cumulative drug release reached 90% after 24 h, which was a significant increase compared to that in the absence of light. This was due to the accelerated degradation of PDA in the acidic environment as a result of the increase in temperature caused by the photothermal effect. The unique drug release property of this composite nanoformulation suggests that its application in cancer treatment can be based on the different needs of patients. The incremental release of drugs can be controlled by administering NIR *in vitro* to produce better therapeutic effects.

The results of the Western blot (WB) experiment are shown in Fig. S5A (Supporting information). Both OXA-DA-siPD-L1@PDA-PEG NPs and OXA-DA-siPD-L1@PDA-PEOz NPs inhibited PD-L1 protein expression in tumor cells to varying degrees, and at pH 5.5, the inhibitory effect of OXA-DA-siPD-L1@ PDA-PEOz on PD-L1 protein expression was further increased. This might be since in a slightly acidic environment, the PEOz-modified nano-system was more easily ingested by tumor cells, with a lysosomal escape effect, thus improving the bioavailability of siPD-L1. The encapsulation of siPD-L1 by the nano-composite system was detected by gel electrophoresis, and the experimental results are shown in Fig. S5B (Supporting information). Compared with the free siPD-L1 which was not encapsulated with the carrier, siPD-L1 was quickly released into the gel, and a clear white band can be seen at the corresponding location. In the OXA-DA-siPD-L1 group, white bands were also observed, indicating leakage of encapsulated siPD-L1 in the nano-system of this group. However, no white bands were observed in the OXA-DA-siPD-L1@PDA, OXA-DA-siPD-L1@PDA-PEG, and OXA-DA-siPD-L1@PDA-PEOz groups, indicating no leakage and that siPD-L1 was well encapsulated in the nano-systems of these three groups.

Systematic evaluations of the photothermal properties of the nanoparticles *in vitro* exposed to an 808 nm NIR irradiation were shown in Figs. 2C–E. As can be seen from Fig. 2C, OXA-DA-siPD-L1@PDA-PEOz with obvious photothermal effect had a more than 17 °C temperature rise under irradiation for 10 min, while pure water has almost no temperature change. Furthermore, the photothermal performances of OXA-DA-siPD-L1@PDA-PEOz aque-

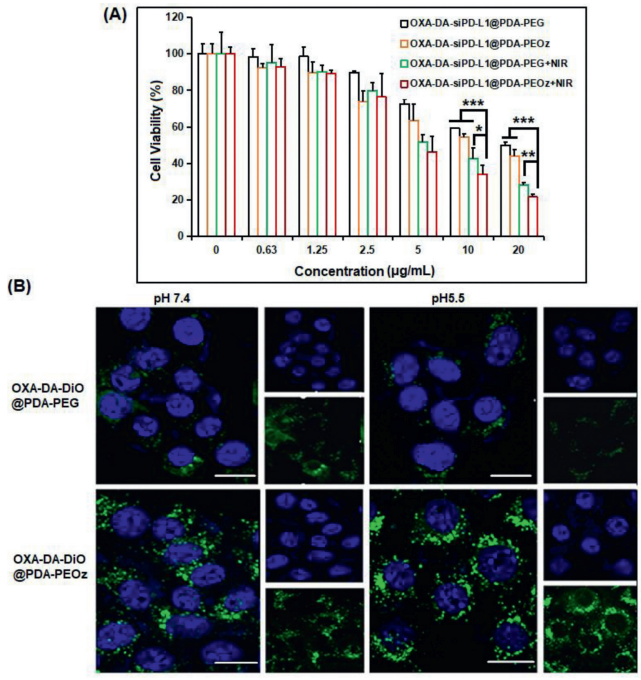


**Fig. 3.** (A) Relative cell viabilities of 4T1 cells for the concentration of different types NPs. Data are mean ± standard deviation (SD), $n = 3$. $^{*}P < 0.05$, $^{**}P < 0.01$, and $^{***}P < 0.005$. (B) CLSM images of 4T1 cells after incubation with OXA-DA-DiO@PDA-PEG and OXA-DA-DiO@PDA-PEOz for 4 h under pH 7.4 and pH 5.5 conditions; scale bar = 10 μm.

ous solution at different concentrations (50–200 μg/mL) had been explored, which showed a strong dependence of OXA-DA-siPD-L1@PDA-PEOz on concentration in Fig. 2D. Photothermal heating curves of OXA-DA-siPD-L1@PDA-PEOz nanoparticles at different power were shown in Fig. S6 (Supporting information), the results showed that the thermal effect of nanoparticles increases with the increase of power. Besides, the photothermal stability of OXA-DA-siPD-L1@PDA-PEOz was verified by four irradiation cycles. As shown in Fig. 2E, there was no significant attenuation of the highest temperature rise during four cycles, indicating good photothermal stability. While the photothermal conversion efficiency of OXA-DA-siPD-L1@PDA-PEOz reached 32.67%, significantly higher than many representative photothermal materials (Fig. S7 in Supporting information).

The cell viability of 4T1 cells was studied using the cell counting kit method. OXA-DA-siPD-L1@PDA-PEG NPs were used to compare with OXA-DA-siPD-L1@PDA-PEOz NPs and the variable of 808 nm NIR irradiation for 10 min was introduced. As can be seen from Fig. 3A, the 4T1 tumor cell inhibitory effect of OXA-DA-siPD-L1@PDA-PEG was lower than that of OXA-DA-siPD-L1@PDA-PEOz, which may be attributable to the ability of OXA-DA-siPD-L1@PDA-PEOz to enhance internalization and lysosome escape through charge reversal in a gradually acidified cell culture medium due to the accumulation of metabolites. After prolonged blood circulation, the OXA prodrug nano-composite delivery system accumulated in the tumor tissues, resulting in enhanced cytotoxicity. In addition, the results of the calcein/propidium Iodide (PI) cell activity and cytotoxicity detection (Fig. S8 in Supporting information) showed that the proportion of dead cells contained in the OXA-DA-siPD-L1@PDA-PEOz + NIR treatment group was the highest. These findings indicate that OXA-DA-siPD-L1@PDA-PEOz can considerably inhibit 4T1 tumor cells when used in combination with photothermal therapy.

To visualize these nanocomposite preparations endocytosed by cancer cells, 4T1 tumor cells incubated with OXA-DA-DiO@PDA-PEG and OXA-DA-DiO@PDA-PEOz for 4 h in different pH media were observed using a confocal laser scanning microscope (CLSM). As shown in Fig. 3B, both of the NPs internalized into the cytoplasm, indicating that OXA-COOH (IV) conjugated on carriers could be endocytosed by cells. OXA-DA-DiO@PDA-PEOz demonstrated a superior cellular uptake of NPs in cells when compared to OXA-DA-DiO@PDA-PEG, which had a lower fluorescence intensity. This may be due to the protonation of PEOz at low pH and the charge inversion on the surface of the nanosystem, leading to an increase in the uptake efficiency. The flow cytometry results reinforce this conclusion (Fig. S9 in Supporting information). We further confirmed this conclusion by assessing zeta potential of OXA-DA-siPD-L1@PDA-PEG and OXA-DA-siPD-L1@PDA-PEOz in different pH media, the results show that, when OXA-DA-siPD-L1@PDA-PEOz NPs is transferred from pH 7.4 medium to pH 5.5 medium, the surface charge changed from negative to positive (Fig. S10 in Supporting information).

The endosome and lysosome escape capacity was estimated by treating 4T1 cells with either OXA-DA-DiO@PDA-PEG or OXA-DA-DiO@PDA-PEOz. After 6 h of incubation. The red NPs and green lysosomes/endosomes merged to produce a yellow fluorescence, suggesting that OXA-DA-DiO@PDA-PEG accumulated within lysosomes and endosomes. Although the OXA-DA-DiO@PDA-PEOz NPs appeared around the cell nucleus, it was distinctly separated from the lysosomes and endosomes by green fluorescence (Fig. S11 in Supporting information). Thus, we concluded that the OXA prodrug nanocomposite delivery system could facilitate the escape of siRNA from lysosomes and endosomes. This phenomenon is attributed to the protonation of PEOz, resulting in the "proton sponge effect", which may cause the lysosome and endosome membranes to rupture, thereby releasing siRNAs into the cytoplasm.

OXA-DA-siPD-L1@PDA-PEOz NPs were subjected to *in vitro* environments at pH 7.4, pH 5.5, and pH 5.5 + NIR, and the morphological changes were observed by TEM after 3 and 7 days to determine its degradation property, the results of which are shown in Fig. S12 (Supporting information). At pH 7.4, after 3 days (Fig. S12A) and 7 days (Fig. S12D) in the simulated *in vitro* environment, the nano-composite system still exhibited a relatively clear granular shape and outline, without obvious degradation. However, at pH 5.5, after 3 days in the simulated *in vitro* environment, no obvious granular morphology could be observed, and the structure of nanoparticles began to collapse (Fig. S12B). After 7 days most of the nanoparticles were degraded, and only a few tiny particles remained, to be cleared completely by the kidneys (Fig. S12E). This indicates that OXA-DA-siPD-L1@PDA-PEOz has good degradability at pH 5.5 compared to pH 7.4. Further, when OXA-DA-siPD-L1@PDA-PEOz was exposed to pH 5.5 and given a one-time NIR light before observation, the presence of tiny particles was observed after only 3 days (Fig. S12C), while after 7 days the presence of OXA-DA-siPD-L1@PDA-PEOz was almost completely unobservable (Fig. S12F). It suggests that the temperature increase induced by 808 nm NIR light further disrupts the structure of the nanocomposite drug delivery system, thereby accelerating the degradation process.

The antitumor activity *in vivo* was assessed by treating 4T1 tumor-bearing mice with various NPs for 20 days and recording changes in tumor volume and body weight. All the protocols for experiments *in vivo* were approved by the Institutional Animal Care and Use Committee of Sun Yat-sen University (Approval No. SYSU-IACUC-2022–001312). The results are shown in Fig. 4. The highest antitumor activity was observed in the OXA-DA-siPD-L1@PDA-PEOz + NIR treatment group. The tumors in this group almost disappeared on the last measurement (Fig. 4A). The body weight changes of mice injected with different NPs showed a steady increase (Fig. S13 in Supporting information), indicating that the NPs had good biocompatibility, while there was no signif-

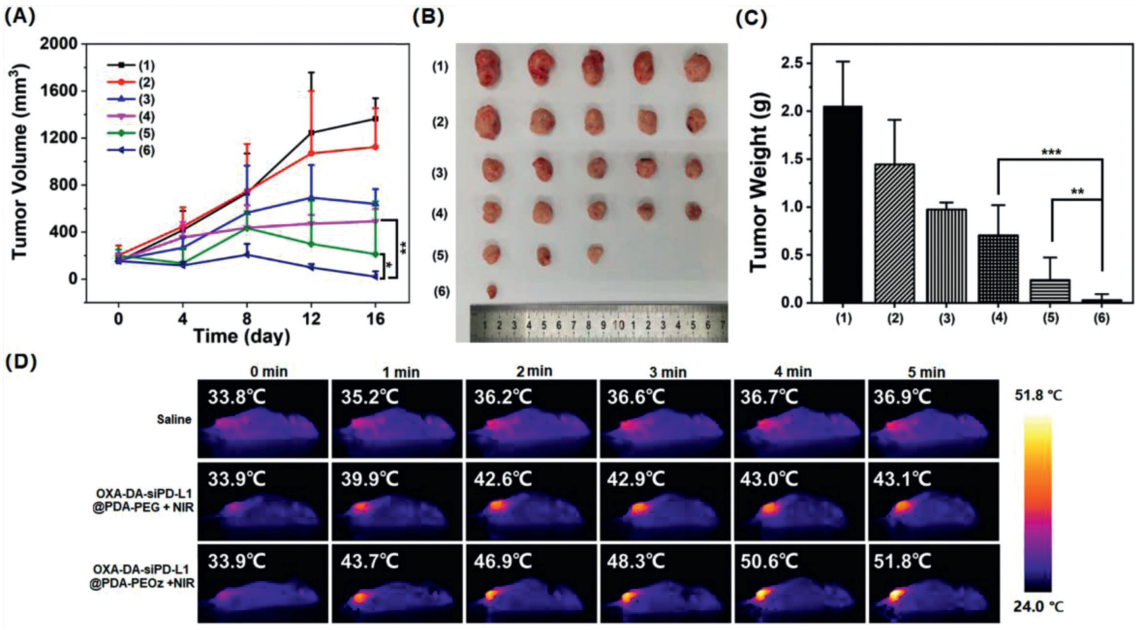


**Fig. 4.** (A) Changes of tumor volumes with different treatments. (B) Morphology of tumors taken from the sacrificed mice in all groups at the 20th day. (C) Tumor weight of each group taken from the sacrificed mice at the 20th day. (D) Evaluation of photothermal effect *in vivo*, Data are mean ± SD, $n = 5$. (1)–(6) represent saline, OXA-DA NPs, OXA-DA-siPD-L1@PDA-PEG, OXA-DA-siPD-L1@PDA-PEOz, OXA-DA-siPD-L1@PDA-PEG + NIR and OXA-DA-siPD-L1@ PDA-PEOz + NIR in this figure, respectively; $^{*}P < 0.05$, $^{**}P < 0.01$, and $^{***}P < 0.005$.

icant difference in body weight among all groups. The difference in antitumor activity was assessed by visual observation of the final excised tumors (Fig. 4B) and weights of these tumors (Fig. 4C). The findings indicate that OXA-DA-siPD-L1@PDA-PEOz can achieve the best enrichment effect through the charge reversal at the tumor site, producing an excellent comprehensive therapeutic effect through the synergistic effect of chemotherapy and photothermal therapy [38,39]. In addition, the proliferation inhibition and apoptosis of tumor cells *in vivo* were investigated by immunohistochemistry (Fig. S14 in Supporting information). The OXA-DA-siPD-L1@PDA-PEOz + NIR treatment group demonstrated superior tumor cell proliferation inhibition effects when compared to the other groups, while a significant proportion of tumor cells underwent apoptosis. Hematoxylin and eosin (H&E) results further confirmed this conclusion.

The performances of infrared thermal imaging *in vivo* were recorded under 808 nm NIR irradiation (Fig. 4D). The group injected with OXA-DA-siRNA@PDA-PEOz showed a remarkable temperature rise within 5 min compared with either the control group or the group injected with OXA-DA-siRNA@PDA-PEG. It was inferred that after PEOz modification, more nanoparticles can achieve long-term circulation and eventually enrich the tumor site, rather than being cleared by the endothelial network system thereby producing a stronger photothermal effect by increasing the local concentration of the tumor site [40].

To evaluate the immune regulatory effect of PD-L1 protein expression, immunohistochemical analysis was used to assess the levels of interferon-$\gamma$ (IFN-$\gamma$), $CD8^+$ T cells, and PD-L1 expression in subcutaneous tumors [41,42]. A decrease in PD-L1 expression was observed in the OXA-DA-siPD-L1@PDA-PEOz treatment group (Fig. S15 in Supporting information). This may be attributable to the increased bioavailability of siPD-L1 due to the lysosomal escape effect of PEOz in tumor tissues. In addition, higher levels of $CD8^+$ T cell infiltration were observed in the OXA-DA-siPD-L1@PDA-PEOz + NIR treatment group. The level of expression of IFN-$\gamma$, an important marker of $CD8^+$ T cell activation, was considerably increased in the OXA-DA-siPD-L1@PDA-PEOz + NIR treatment group. Notably, the level of expression of TNF-$\alpha$ decreased significantly in the OXA-DA-siPD-L1@PDA-PEOz + NIR treatment group, and the level of expression of interleukin-10 (IL-10) increased significantly in this group (Fig. S16 in Supporting information). These findings indicate that the specific inhibition of PD-L1 protein expression by siPD-L1 can enhance the activation and infiltration of T cells in tumor tissues to achieve an antitumor effect [43,44].

To further evaluate the safety of the nanomedicines, H&E staining was performed on the heart, liver, spleen, lung and kidney, and the microscopic observation results were shown in Fig. S17 (Supporting information). There was no obvious damage to the tumor tissue in the treatment groups, indicating that the synergistic chemo/photothermal/immunotherapy caused no damage to the tumor tissues and thus had the best therapeutic effect. Also, there were no obvious pathological changes in the main organs of each group, which showed that nanoplatforms are safe [45].

In conclusion, PEOz-modified multifunctional biodegradable nanoplatform was successfully formulated for loading OXA and siPD-L1 in a synergistic chemo/photothermal/immunotherapy. The OXA-DA-siPD-L1@PDA-PEOz NPs could release drugs rapidly and easily biodegrade with the assistance of exogenous NIR, and specifically degraded PD-L1 protein in tumor cells and produced excellent antitumor effects with high safety *in vivo*.

## Declaration of competing interest

The authors declare that they have no known competing financial interests or personal relationships that could have appeared to influence the work reported in this paper.

## Acknowledgments

We are grateful for the financial support from the National Natural Science Foundation of China (Nos. 32071342 and 32101065), the Natural Science Foundation of Guangdong Province (Nos. 2023A1515012015, 2022A1515110271 and 2020A1515011353).

## Supplementary materials

Supplementary material associated with this article can be found, in the online version, at doi:10.1016/j.cclet.2023.108346.

## References


[1] F. Bray, J. Ferlay, I. Soerjomataram, et al., CA Cancer J. Clin. 68 (2018) 394–424.
[2] J.M. Chen, T. Qiud, M.G. M.auk, et al., Chin. Chem. Lett. 33 (2022) 4126–4132.
[3] R.L. Siegel, K.D. Miller, H.E. Fuchs, CA Cancer J. Clin. 72 (2022) 7–33.
[4] C. Xia, X. Dong, H. Li, et al., Chin. Med. J. 135 (2022) 584–590.
[5] Y.K. Y.u, Q.Z. Cheng, X.Y. Ji, et al., Sci. Adv. 8 (2022) eadd3599.
[6] R. Fritsch, J. Hoeppner, Expert Rev. Gastroenterol. Hepatol. 13 (2019) 285–291.
[7] J. Yang, D.H. Dai, L.J. Ma, et al., Chin. Chem. Lett. 32 (2021) 729–734.
[8] K. Sałat, Pharmacol. Rep. 72 (2020) 508–527.
[9] B. Feng, F. Zhou, B. Hou, et al., Adv. Mater. 30 (2018) e1803001.
[10] W.Q. Lim, G.B. Yang, S.Z.F. Phua, et al., ACS Appl. Mater. Interfaces 11 (2019) 16391–16401.
[11] L. Song, Y. Hao, C.J. Wang, et al., J. Control. Release 350 (2022) 922–932.
[12] Y.J. Huang, Z.L. Guan, X.L. Dai, et al., Nat. Commun. 12 (2021) 4310.
[13] N.D. V.olkow, J.S. Fowler, G.J. Wang, Neuropharmacology 56 (2009) 3–8.
[14] A.J. Langdon, N.D. Daw, Trends. Cogn. Sci. 24 (2020) 499–501.
[15] Q. Guan, R. Guo, S. Huang, et al., J. Control. Release 320 (2020) 392–403.
[16] M. Zhu, Y. Shi, Y. Shan, et al., J. Nanobiotechnology 19 (2021) 387.
[17] D. Wu, J. Zhou, X. Chen, et al., Biomaterials 238 (2020) 119847.
[18] Y. Wu, Y. Huang, C. Tu, et al., Nanoscale 13 (2021) 6439–6446.
[19] S. Acter, M.L.P. Vidallon, J.P. King, J. Mater. Chem. B 9 (2021) 8962–8970.
[20] W.F. Zeng, Z.M. Li, H.Z. Chen, et al., Cell. Rep. Phys. Sci. 3 (2022) 100898.
[21] Z.M. Li, Y.K. Yu, W.F. Zeng, et al., Small 18 (2022) 2201803.
[22] W. Cheng, X. Zeng, H. Chen, et al., ACS Nano 13 (2019) 8537–8565.
[23] Y.L. J.i, B.X. Gu, S.J. Xie, et al., Adv. Mater. 33 (2021) e2102292.
[24] M. Dirauf, N. Fritz, M. Gottschaldt, Macromol. Rapid. Commun. 42 (2021) e2100132.
[25] R. Lima-Sousa, C.G. A.lves, B.L. Melo, et al., Mater. Sci. Eng. C: Mater. Biol. Appl. 130 (2021) 112468.
[26] R.G. Thomas, S.P. Surendran, Y.Y. Jeong, Front. Mol. Biosci. 7 (2020) 610533.
[27] Z.M. Li, Y. Yang, H.X. Wei, et al., J. Control. Release 338 (2021) 719–730.
[28] J. Mao, J. Li, J. Ding, Acta Pharm. Sin. 52 (2017) 1235–1240.
[29] N. Jia, W.P. Li, D. Liu, et al., Mol. Pharm. 17 (2020) 1516–1526.
[30] T. Frankel, M.P. Lanfranca, W. Zou, Adv. Exp. Med. Biol. 1036 (2017) 51–64.
[31] V. Velcheti, K. Schalper, Am. Soc. Clin. Oncol. Educ. Book 35 (2016) 298–308.
[32] R.S. Riley, C.H. June, R. Langer, Nat. Rev. Drug Discov. 18 (2019) 175–196.
[33] F. Xie, M. Xu, L. Lu, Mol. Cancer 18 (2019) 146.
[34] L. Jia, Y. Gao, T. Zhou, et al., Biomaterials 271 (2021) 120711.
[35] K. Kim, S.A. Yuk, A.M. Dieterly, et al., ACS Nano 15 (2021) 4576–4593.
[36] P.S. Hegde, D.S. Chen, Immunity 52 (2020) 17–35.
[37] H. Yao, J. Lan, C.S. Li, et al., Nat. Biomed. Eng. 3 (2019) 306–317.
[38] Z.M. Li, X.T. Shan, Z.D. Chen, et al., Adv. Sci. 8 (2021) 2002589.
[39] P. Huang, D.Z. Lian, H.L. Ma, et al., Chin. Chem. Lett. 32 (2021) 3696–3704.
[40] Z.M. Li, Q.Y. Liu, Y. Zhang, et al., Drug Deliv. 28 (2021) 700–708.
[41] Q.Q. Xiao, X.T. Li, C. Liu, et al., Acta Pharm. Sin. B 13 (2023) 3503–3517.
[42] X.Q. Du, Y.Q. Hou, J. Huang, et al., Acta Pharm. Sin. B 11 (2021) 3272–3285.
[43] G.F. Boafo, Y.J. Shi, Q.Q. Xiao, et al., Chin. Chem. Lett. 33 (2022) 4600–4604.
[44] J.P. S.heng, J.C. Wu, C.H. Yin, et al., Chin. Chem. Lett. 34 (2023) 107738.
[45] N.N. Li, Y. Liu, X.Y. Ji, et al., Chin. Chem. Lett. 32 (2021) 3787–3792.